City and Environment Interactions 27 (2025) 100201

Contents lists available at ScienceDirect

City and Environment Interactions

journal homepage: www.sciencedirect.com/journal/city-and-environment-interactions

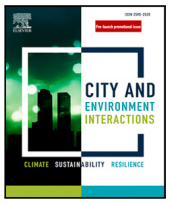

Research articles

Urban fluxes for free: Estimating urban turbulent surface fluxes from crowdsourced meteorological canyon layer observations

W. van der Meer, F. Zantinge, G.J. Steeneveld *

Meteorology and Air Quality Section, Wageningen University, P.O. box 47, Wageningen, 6700 AA, The Netherlands

ARTICLE INFO

Dataset link: https://maq-observations.nl/data-downloads/, https://www.knmi.nl/nederland-nu/klimatologie/uurgegevens, https://dev.netatmo.com/apidocumentation/weather#getstationsdata, https://dev.netatmo.com/legal

Keywords:
Crowdsourcing
Urban surface fluxes
Amsterdam
Netatmo
Surface energy balance
Solar radiation

ABSTRACT

Crowdsourcing and citizen science data have gained insight in the urban heat island effect and intra-urban heat patterns in many cities. However, while the urban energy balance is key in understanding the urban climate, professional urban surface flux measurements are relatively scarce. Here we develop a method to estimate urban fluxes of sensible heat, latent heat and momentum using solely crowdsourced temperature, humidity and wind speed observations in the urban canopy through Netatmo amateur weather stations. Also, the spatial variance of temperatures recorded in a network of Netatmo stations (varT) appears to be a good predictor for the incoming solar radiation. The proposed flux method is evaluated against eddy covariance flux estimates in Amsterdam (The Netherlands), and appears to have a median absolute error of 46.3 Wm^{-2} and 22.8 Wm^{-2} for sensible and latent heat flux respectively. When applying varT these values drop to 30.5 and 17.5 Wm^{-2} respectively. These scores compare well with schemes driven by professional observations. Hence, we offer a meaningful flux scheme that runs purely on free observations.

1. Introduction

Urban areas are rapidly expanding and 68% of the world population is expected to reside in cities in 2050 [1]. Simultaneously, climate change increases the human heat load, especially in cities, which are disproportionately affected by the urban heat island (UHI) effects [2]. Consequently, urban areas are expected to see a rise in the detrimental health effects associated with heat stress [3–5].

Despite the urban heat stress, the prevalence of high-quality urban meteorological observations does not suffice to fully understand the highly variable temperatures in urban areas [6]. Advanced understanding of urban climates requires extensive urban meteorological measurement networks [7,8]. However, most observations serve synoptic-scale meteorology and omit relatively small-scale city effects [9]. Underrepresentation in urban areas is due to extensive siting requirements for observations, vandalism risk, and the avoidance of cities by professional networks because more homogeneous surfaces are required for standardised observations [6,10].

Turbulent heat fluxes govern the urban surface energy balance and surface temperature [11]. Previous studies explored the urban energy balance to understand the drivers behind the UHI in selected cities that were diverse in size, culture, economic status and climate [12,13]. However, generalising flux models remains challenging since it requires flux observations of latent heat (Q_e) and sensible heat (Q_h). The spatial density of flux observations is even lower than for routine weather data, because of their relatively high costs and demanding siting requirements.

The high population density in cities provides plenty of opportunity for acquiring citizen data [14]. For example, Netatmo maintains a worldwide and spatially dense weather station network of basic at-home atmospheric sensors. Its data has widely enhanced meteorological analyses by increasing the spatial density of observations [e.g. 15] for temperature [e.g. 16–18] for wind [e.g. 19,20], and precipitation [21–24]. Crowdsourced observations from sources other than Netatmo have also been insightful for urban climates studies [e.g. 25–29]. These types of citizen data can provide valuable information on temperature, wind, humidity, and precipitation, but crowdsourced weather observations typically do not involve surface energy fluxes.

Holtslag and Van Ulden [30] and De Rooy and Holtslag [31] developed a scheme to estimate the surface energy fluxes over grassland from standard screen-level weather data. Although earlier studies have estimated urban surface fluxes from professional routine weather observations [32,33], none have done this from crowdsourced observations in urban canopies alone. This study extends their methods to estimate neighbourhood-scale urban turbulent heat fluxes, using only crowdsourced Netatmo observations in the urban canopy, supplemented with professional radiation observations.

* Corresponding author.
E-mail address: gert-jan.steeneveld@wur.nl (G.J. Steeneveld).

https://doi.org/10.1016/j.cacint.2025.100201
Received 4 November 2024; Received in revised form 13 February 2025; Accepted 22 April 2025
Available online 9 May 2025

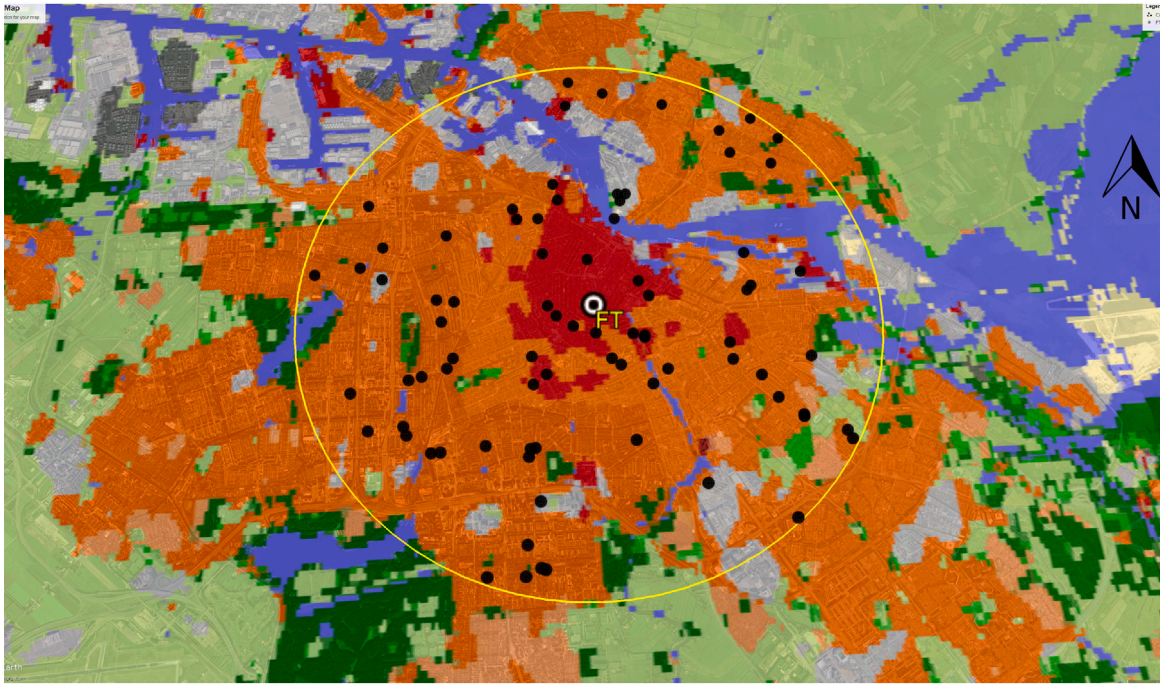

Fig. 1. Local Climate Zome Map of Amsterdam (source: https://lcz-generator.rub.de/), indicating 81 Netatmo stations that provided data in the study period. The study area has a radius of 5 km (yellow circle) around the flux tower (indicated by FT). Background data from GoogleEarth [34]. (For interpretation of the references to colour in this figure legend, the reader is referred to the web version of this article.)

Moreover, we develop a novel method to estimate incoming shortwave radiation ($K^{\downarrow}$) from the spatial variability of the basic Netatmo temperature observations alone, effectively allowing the proposed flux model to be applied to any urban area with sufficient Netatmo stations, independent of the availability of professional solar radiation observations.

The $K^{\downarrow}$ estimation builds on the effect that the spatial temperature variance within a Netatmo network increases when the $K^{\downarrow}$ increases [35]. The underlying idea is that always some stations are non-ideally placed and can be directly exposed to sunlight, and their temperature recordings will deviate positively from other stations [36]. This increases the instantaneous spatial temperature variance in the Netatmo network. As Netatmo is a crowdsourced dataset, we may reasonably assume a substantial share of the stations is exposed to direct solar radiation [16]. Previous work on the radiation bias in Netatmo temperature readings has predominantly been focused on removing stations affected by radiation errors [16,37]. However, if enough radiation-biased stations are present in an area, they can provide useful information on $K^{\downarrow}$.

Below, Section 2 presents the data acquisition and quality assessment procedures, the urban flux model, and the $K^{\downarrow}$ estimation method from Netatmo data. Section 3 presents the model results using professionally observed radiation data, and offers proof-of-concept of the $K^{\downarrow}$ estimation method. Subsequently, the $K^{\downarrow}$ estimation is implemented into the model. Sections 4 and 5 contain the Discussion and Conclusions.

2. Methods

2.1. Site description

Amsterdam is the Dutch capital, located between the North Sea and the Marker Lake, and at 2 m below sea level. The Netherlands has a temperate oceanic Cfb climate with a annual mean 2-m air temperature of 10.5 °C, a annual mean precipitation of 851 mm, and prevailing southwesterly winds. The study period contains January 1st–August 31st 2022. With an average temperature of 12.3 °C during the study period, it was 0.9 °C warmer than normal. The study period had 1729 sun hours (27% above normal), and 392 mm precipitation (110 mm below normal).

The city centre is characterised by three-storey buildings, canals and narrow streets, and is surrounded by residential areas with three- and four-storey houses [38]. We use eddy covariance (EC) flux tower observations taken on a rooftop (40 m above ground) at 52.366548°N, 4.893020°E, in the historic city centre (instrument details below). The EC tower is part of the Amsterdam Atmospheric Monitoring Supersite (AAMS, [39]). Netatmo data are collected in an area of 5 km around the EC tower (Fig. 1). Also, we use automated weather station data from Amsterdam Airport (WMO code 06240; at 52.31541°N, 4.790223°E) at 9.2 km southwest of the flux tower.

2.2. Instrumentation and data

We employ a CSAT3 (Campbell Scientific) sonic anemometer. The data from this instrument were processed with a 30 min averaging interval with the EddyPro Software, and are labelled with a quality indicator 0, 1 or 2, indicating high, intermediate or poor quality, respectively [40]. The dataset contains sensible and latent heatflux and friction velocity, and is available from [41], who have gap-filled and harmonised 20 different urban flux observation datasets. We refer to their work for the details on the processing of the flux data.

2.3. Acquisition of Netatmo data

Netatmo offers an extensive worldwide at-home observation network, in which users can voluntarily opt-in to share their data on the Netatmo online platform. A Netatmo setup consists of an outdoor temperature and humidity module, and indoor air quality, atmospheric pressure and noise modules. We also use setups containing the anemometer extension.

The Netatmo system contains a Sensirion SHT20 sensor chip (Sensirion AG, Stäfa, Switzerland) for temperature readings [15]. The aluminium casing is passively ventilated, making it prone to radiation

Table 1
Data quality levels of Netatmo data in Amsterdam. Indicated are the remaining percentages of the original possible data locations.

Level	Description	(N = 95)
A0	Temperature data with correct timestamp	100%
A1	Stations with unique coordinates	85.3% (N = 81)
A2	80% hourly data per day	83.5%
A3	80% daily data per month	75.7%
B	Indoor station filter	71.2%

bias [42]. Temperature is recorded every 6 s and is aggregated in steps of 5 min in a range of −40 °C to 65 °C, with an accuracy of 0.3 K. The wind module is a cylindrical sonic anemometer with 4 ultrasonic transducers, with a range of 0–45 ms^{-1} with an accuracy of 0.5 ms^{-1}.

The Netatmo network has high spatial coverage in cities, where traditional measurement stations are underrepresented [29]. The station density was about 0.85 km^{-2} in Amsterdam in 2019 [37]. A disadvantage of the Netatmo network is that the sensors are managed by volunteers, which raises questions about siting quality. The relatively large share of erroneous observations requires thorough quality assessment and quality control before the results are trustworthy. Such procedures have been established by Meier et al. [16] and Fenner et al. [37], making Netatmo data suitable for our research.

We used the *Getstationdata* API provided by Netatmo to download all historical and current Netatmo stations in Amsterdam. The data was stored for each Netatmo station individually. Since the stations do not record synchronously, the data was in random intervals of about 5 min. Since we are interested in the local scale fluxes, the data was resampled to fixed 30 min time steps, averaging all observations 30 min before the time step (see e.g. [43]). A 30 min resolution was also selected to match the time interval of radiation data in Amsterdam. The procedure was similar to [37].

These records were subjected to quality checks A1, A2, A3 and B in [16]. After these quality checks, the number of available stations with sufficient data quality varied between 52 and 63 stations throughout the study period. Table 1 summarises the quality checks and their implication for data availability.

Quality check A1 ensures that all location metadata is unambiguous. Stations for which the latitude and longitude are exactly equal, are both removed from the dataset. This step removed 15% of the data from the dataset, which is relatively high. Nevertheless, we stick to this approach since the final amount of available data points exceeds the minimum required of about 36 stations (see Discussion section). Quality check A2 removes, for each station individually, all days for which there is less than 80% of the raw data available, for 24 h of 5 min intervals (maximum 288 recordings) the required number of half-hour measurements is 230. This ensures the intra-daily quality of the temperature data. Quality check A3 removes in a similar fashion each month that produced less than 80% correct daily data.

In quality level B a minimum temperature that deviates too much from the mean is suspected of being placed inside, and thus does not provide useful meteorological information. When in a given month, the average daily minimum temperature for a station differed over 1.5 standard deviations from the mean of all stations, the station's data for that month was removed from the dataset.

From the Netatmo wind data, only the wind speed observation was used at times with valid temperature readings. In the study period, 19 out of the 81 stations with unique coordinates included wind modules. The wind direction of the Netatmo data is prone to the effects of the local morphology of the placement of the module [19], so it is disregarded. Moreover, the directional component is not required for the numerical modelling framework proposed in this research.

2.4. Estimation of $K^{\downarrow}$ from Netatmo observations

Netatmo half-hourly data with level B within 5 km from the flux tower site were used to estimate the variance in temperature observations (varT in K^2). Subsequently, varT was related with the blocked fraction of the global radiation at the location of the flux tower ($f_{cc}^{\downarrow}$), i.e. the fraction of the clear-sky incoming shortwave radiation ($K_{cs}^{\downarrow}$) that does not reach the surface. As clouds have a reflective and scattering effect on global radiation, the $f_{cc}^{\downarrow}$ is closely related to cloud cover. Note that there is not a 1:1 correlation, as the effect of clouds on $K^{\downarrow}$ is complex and non-linear [44]. Eqs. (1a) and (1b) summarise the relations.

$$K_{cs}^{\downarrow} = K_{toa}^{\downarrow} * (1 - f_{clear}^{\downarrow}) \tag{1a}$$

$$K^{\downarrow} = K_{cs}^{\downarrow} * (1 - f_{cc}^{\downarrow}) \tag{1b}$$

$K_{toa}^{\downarrow}$ shortwave downwelling radiation at the top of the atmosphere (Wm^{-2})

$K_{cs}^{\downarrow}$ surface shortwave downwelling radiation in completely cloudfree conditions (Wm^{-2})

$K^{\downarrow}$ actual incoming shortwave radiation at the surface (Wm^{-2})

$f_{clear}^{\downarrow}$ fraction loss of $K^{\downarrow}$ in clear conditions (≈ 0.2)

$f_{cc}^{\downarrow}$ fraction loss of $K^{\downarrow}$ because of cloud cover

$K_{toa}^{\downarrow}$ was parameterised for each 30 min time step, depending on the day-of-year and coordinates using R-package *solaR* [45]. Then $f_{clear}^{\downarrow}$ was used, which is defined as the fraction of the $K_{toa}^{\downarrow}$ that is reflected and scattered by the atmosphere. We used $f_{clear}^{\downarrow} = 0.2$, which is equal to the value as used by De Rooy and Holtslag [31].

The relation between incoming solar radiation and varT was investigated using least-squares regression on dimensionless regression parameters γ and δ of Eq. (2). The regression uses a log-transformed varT data, since the preliminary results indicated that the relation is non-linear in varT:

$$f_{cc}^{\downarrow} = \gamma + \delta \ln(\text{varT}) \tag{2}$$

VarT of all temperature stations in a 5 km radius around the Amsterdam urban flux tower for the period March 1 to August 31 of 2020 (8832 entries) were related to the $f_{cc}^{\downarrow}$, and the outcome will be discussed in more detail in Section 3.

2.5. Model formulation

The surface radiation and energy budget form the basis of the flux model [30]. When available, professional $K^{\downarrow}$ observations can directly feed into the model. Without professional data, $K^{\downarrow}$ can be estimated from varT (Section 2.4).

$$Q_* = K^{\downarrow} + L^{\downarrow} - K^{\uparrow} - L^{\uparrow} \tag{3a}$$

$$L^{\downarrow} = \epsilon_{\text{air}} \sigma T_{\text{air}}^4 + c_2 \text{CC} \tag{3b}$$

$$K^{\uparrow} = \alpha K^{\downarrow} \tag{3c}$$

$$L^{\uparrow} = \epsilon_{\text{surf}} \sigma T_{\text{surf}}^4 + \left(1 - \epsilon_{\text{surf}}\right) L^{\downarrow} \tag{3d}$$

Q_* Net radiation (Wm^{-2})

σ Stefan–Boltzmann constant ($5.67 \cdot 10^{-8}$ $Wm^{-2}K^{-1}$)

c_2 Empirical parameter of 60 Wm^{-2} [30]

CC Cloud cover (related to $f_{cc}^{\downarrow}$)

α Surface albedo (0.15 based on AAMS observations)

T_{air} Air temperature (K)

T_{surf} Surface temperature (K)

$\epsilon_{\text{air}}, \epsilon_{\text{surf}}$ Emissivity of the air and the surface (1.0)

Table 2
Land surface types and cover fractions (f_i) in a 5 km radius around the flux tower station, and used in the OHM based on their sources.

	f_i	a_1 (–)	a_2 (h)	a_3 (Wm^{-2})	Source
Buildings	0.45	0.48	0.34	−33.9	Yap [46]
Water	0.15	0.50	0.21	−39.1	South et al. [47]
Vegetation	0.15	0.22	0.33	−19.9	Doll et al. [48]
Canyons	0.05	0.68	0.30	−42.4	Narita [49]
Pavement	0.20	0.68	0.30	−42.4	Narita [49]

The available energy (Q_a) follows from Eq. (4a), while the storage heat flux is estimated through Eq. (4b), originating from the Objective Hysteresis Model [50]. This model estimates the heat storage in the urban fabric of different land use areas and their fraction. In the OHM, coefficients a_1, a_2 and a_3 are weighted by their land cover fraction f_i in the footprint (Table 2).

$$Q_a = Q_* - Q_s \tag{4a}$$

$$Q_s = \sum_{i=1}^{n} \left(f_i a_{1i} Q_* + f_i a_{2i} \frac{\partial Q_*}{\partial t} + f_i a_{3i} \right) \tag{4b}$$

The Q_a is then partitioned into Q_e and Q_h with the [51] concept. The necessary slope of the saturated vapour pressure curve (s) and the psychrometer constant (γ) are computed with Eq. (5c) [52] and (5d) [53].

$$Q_e = a \frac{s}{s+\gamma} \left(Q_* - Q_s \right) + b \tag{5a}$$

$$Q_h = \frac{(1-a)s+\gamma}{s+\gamma} \left(Q_* - Q_s \right) - b \tag{5b}$$

$$s = 0.2\Big(0.00738(T_{\text{air}} - 273.15) + 0.8072\Big)^7 - 0.000116 \tag{5c}$$

$$\gamma = \frac{c_p}{L} \tag{5d}$$

a Empirical parameter(determined with Eq.(6))
b Empirical parameter with value 3 see [54]
s Slope of the saturated vapour pressure curve (kPa K^{-1})
γ Psychrometric constant (kPa K^{-1})
c_p Specific heat capacity for dry air (J kg^{-1} K^{-1})
L Obukhov length (m)

The model as a whole is sensitive to parameter values of a. To make the model adaptable for use in different cities, a depends on the surface cover types (Table 2) within the footprint of the flux tower, based on [33]:

$$a = 0.3 f_b + f_w + 1.2 f_v + 0.5 f_c + 0.5 f_p \tag{6}$$

with the surface cover fraction of buildings (f_i), water (f_w), vegetation (f_v), urban canyons (f_c) and pavement (f_p). Because T_{surf} (Eq. (8a)) is dependent on the temperature scale (T_*) and the Obukhov length (L), which in turn depends on Q_h and u_*, T_{surf} is solved iteratively with start values of L=10^6 m, β=0.3 (see next section) and T_*=0 K.

Each iteration starts with estimating u_* with Eq. (7a), which requires wind speed (u_h) at mean building height (z_h) (Eq. (7b)). The necessary length scale l_m and L_c are calculated with Eqs. (7c) and (7d). Estimating L_c requires the plan area index (λ_p) and frontal area index (λ_f), which are set to 0.4 and 0.16 respectively for Amsterdam [55].

$$u_* = \beta u_h \tag{7a}$$

$$u_h = u / \exp\left(\frac{(h - z_h)\,\beta}{l_m} \right) \tag{7b}$$

$$l_m = 2\beta^3 L_c \tag{7c}$$

$$L_c = \frac{1-\lambda_p}{\lambda_f} \frac{2 z_h}{c_d} \tag{7d}$$

u_* Friction velocity (ms^{-1})
u_h, u Wind speed at mean building height z_h and observation height h (ms^{-1})
h Observation height from the surface (mean of Netatmo stations) (m)
z_h Mean building height from the surface (m)
β Harman-Finnigan parameter [56]
l_m Mixing length (m)
L_c Canopy penetration depth (m)
λ_p, λ_f Plan area index and frontal area index
c_d Drag coefficient, fixed value of 1.2 [57]

Then, with a vertical profile based on [56], a new T_{surf} is computed in Eq. (8a). Canopy height temperature (T_h) is found with Eq. (8b). Both formulas require the Prandtl number (Pr) and parameter f to determine the within-canopy profile, which are computed with Eqs. (8c) and (8d) respectively.

$$T_{\text{surf}} = T_h + \frac{Pr}{\beta f} T_* \exp\left(\beta f \frac{-z_h}{l_m} \right) - \frac{Pr}{\beta f} T_* \tag{8a}$$

$$T_h = T_{\text{air}} - \frac{Pr}{\beta f} T_* \exp\left(\beta f \frac{h - z_h}{l_m} \right) + \frac{Pr}{\beta f} T_* \tag{8b}$$

$$Pr = 0.5 + 0.3 \tanh\left(2 \frac{L_c}{L} \right) \tag{8c}$$

$$f = 0.5\sqrt{1 + 4 St Pr} - 0.5 \tag{8d}$$

T_h Air temperature at mean building height (K)
Pr Prandtl number
f Parameter of the within-canopy T profile
St Stanton number, with a fixed value 0.1

Finally, new estimations are made for L, β and T_* with Eqs. 9a-c for the next iteration. If the new L differs less than 1% from the previous value, the iteration is stopped.

$$L = -\frac{\rho c_p u_*^3 T_{\text{air}}}{\kappa g Q_h} \tag{9a}$$

$$\beta = \frac{\beta_N}{\phi_m\left(\frac{\beta^2 L_c}{L} \right)} \tag{9b}$$

$$T_* = -\frac{Q_h}{\rho c_p u_*} \tag{9c}$$

ρ Air density, fixed value of 1.22 kg m^{-3}
κ Von Kármán constant, fixed value of 0.4
g Gravitational acceleration (9.81 ms^{-2})
β_N β in neutral conditions, fixed value of 0.4
ϕ_m Monin–Obukhov similarity theory stability function for momentum [56]

3. Results

We first present the model results when forced with professional radiation data from Amsterdam airport, and Netatmo data for T and u. The second section presents the results when $K^{\downarrow}$ is estimated from Netatmo data.

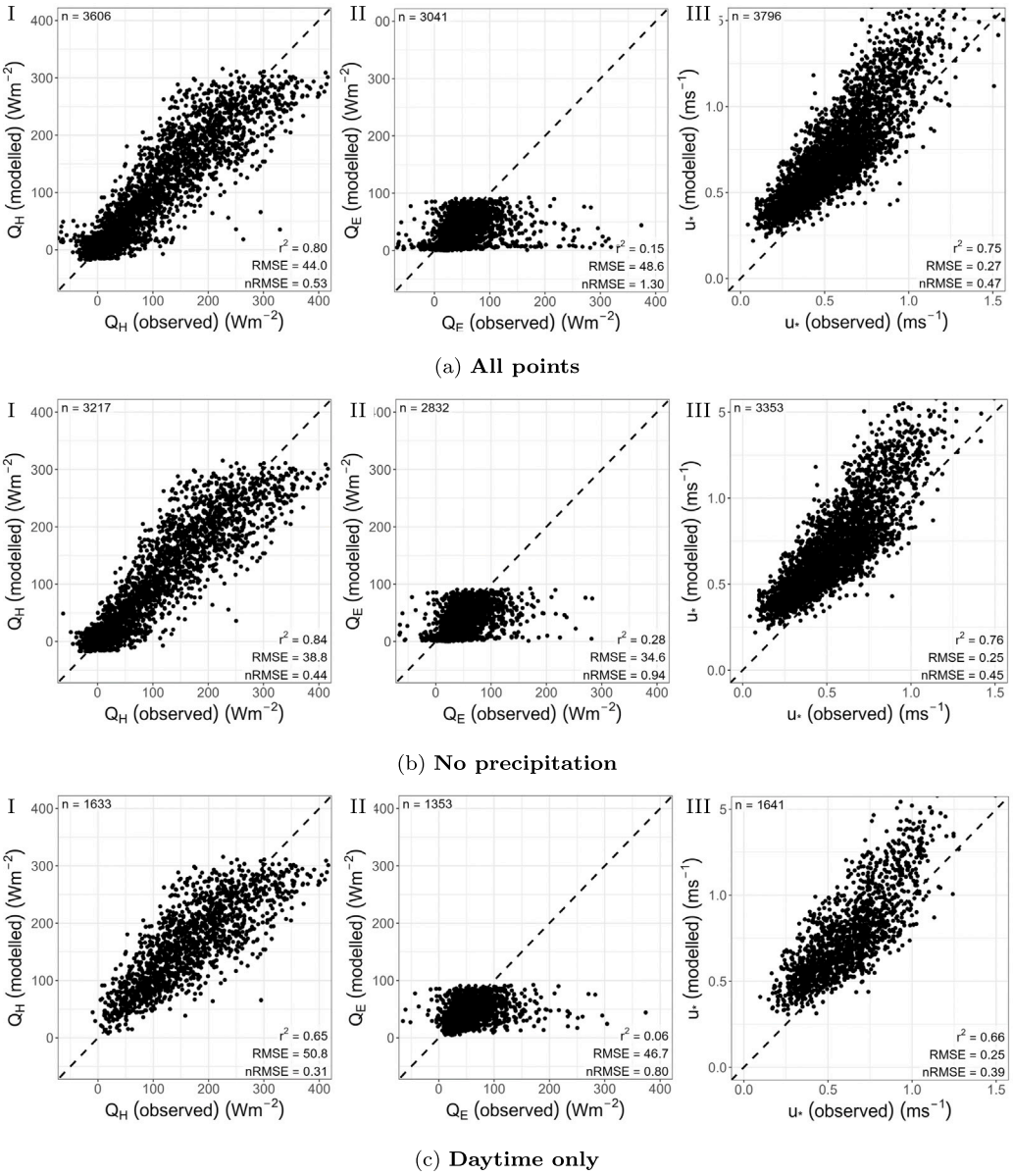

Fig. 2. Observed vs modelled Q_h (I), Q_e (II) and u_* (III) for January 2022 to August 2022 with measured $K^{\downarrow}$ (Amsterdam Airport) and input data from the Netatmo PWSs. For (a), all data points are used. For (b), only points with $P = 0$. For (c), only hours with $K^{\downarrow}_{pot} > 120$ Wm^{-2} (daytime hours). The dashed line indicate the 1:1 relation.

3.1. Model results

First, three experiments are performed in which, Netatmo observations (T and u) are supplemented by professionally measured radiation observations (K and N) from Amsterdam airport. The first experiment includes all data points in the dataset that passed quality control (Fig. 2(a)). The second experiment includes only hours without precipitation (Fig. 2(b)). The third experiment includes only time slots with $K^{\downarrow}_{pot} >$ 120 Wm^{-2}, which are daytime hours only Fig. 2(c).

Fig. 2(a) shows the observed versus the modelled Q_h, Q_e and u_* for the run without data restrictions. The model is able to simulate Q_h, considering the r^2 of 0.80. Nonetheless, the normalised RMSE (nRMSE) of 0.53 reveals that the RMSE of 44.0 Wm^{-2} is relatively high, with respect to the mean flux. Fig. 2(a)-II shows the estimated Q_e differs from the observed Q_e, given the r^2 of 0.15, RMSE of 48.6 Wm^{-2} and nRMSE of 1.29. The modelled u_* is in good agreement with the observations (Fig. 2(a)-III). r^2 amounts to 0.75, and the RMSE of 0.27 ms^{-1} is smaller than half of the mean of u_*, indicated by the nRMSE of 0.47.

When excluding hours with precipitation (Fig. 2(b)), we find a higher r^2 and lower RMSE and nRMSE for Q_h and Q_e. Also for u_*, the r^2 improved, whereas the RMSE and nRMSE remained approximately the same. The improvement for Q_e (Fig. 2(b)-II) in this run is likely due to the dry conditions that are represented better by the fixed Priestley and Taylor [51] parameters a and b than wet conditions. Nevertheless, the model is still not able to simulate Q_e sufficiently and therefore, the fixed moisture availability by means of a and b can only partly explain the poor model performance for Q_e. Another explanation might be that moisture release, for example from vehicle exhausts, air conditioning outlets and chimneys (mainly in winter), has a relatively large effect on Q_e due to the small magnitude of this flux, which is not simulated in the model.

When we focus our analysis on daytime hours only (Fig. 2(c)), r^2 shows lower values for all fluxes, however, a comparison between daytime and nighttime reveals that the model performs better during the day (not shown). Once more, the improvement for the nRMSEs is remarkable, as the nRMSE equals 0.31 for Q_h, 0.80 for Q_e and 0.39 for u_*, even though the RMSEs have not changed much. Again, this

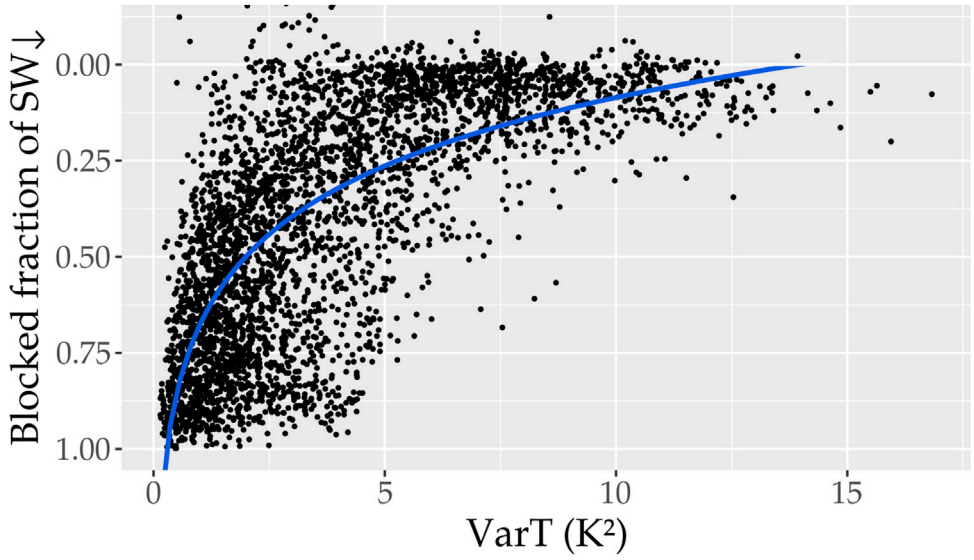

Fig. 3. varT of all temperature stations in a 5 km radius around the flux tower plotted against the $f_{cc}^{\downarrow}$. The blue line indicates a logarithmic least-squares fit regression (Eq. (2) and Table 3). (For interpretation of the references to colour in this figure legend, the reader is referred to the web version of this article.)

can be explained by the inability of the model to simulate the complex nocturnal situation.

3.2. $K^{\downarrow}$ estimation from Netatmo data

Here we introduce a new opportunistic sensing method to extract global radiation from Netatmo temperature sensors. The model is tested for proof-of-concept first, and subsequently the new method is implemented in the flux estimation model.

A three-day period in June 2022 was selected for the first analysis, because of the mix of cloudy and cloudless days. The first day (June 22nd) was completely sunny and dry at Amsterdam airport (Fig. 4), with a mean maximum temperature of about 25 °C for all Netatmo stations. There was a northeasterly mean 10-m wind speed of 2.8 ms^{-1}. Because of the sunny conditions, some stations showed large temperature deviations from the average in the network on this day and were assumed to be radiation-biased on this day.

June 23rd was mostly sunny with a T_{max} of approximately 30 °C and a northeasterly mean wind speed of 3.3 ms^{-1}. Some clouds formed later in the day, lowering the varT. June 24th was a partially cloudy day, with a T_{max} of 24 °C and a southwesterly mean wind speed of 3.5 ms^{-1}.

In general, the varT follows a pattern similar to that of daily sunshine duration, but also a sub-daily relation is distinguished. June 23 and June 24 were cloudy for a fraction of the day. In these cases, the varT follows a pattern that resembles the diurnal pattern of the sunshine duration. In other words, the varT follows the sunshine duration also when a fraction of the day is cloudy. This suggests that the VarT approach can also provide intra-daily data on $K^{\downarrow}$.

We find a distinct relation between sunshine duration and varT in the Netatmo dataset. Fig. 5 shows that for hours with a longer sunshine duration, the varT is higher than for hours with a short sunshine duration, signalling a positive relation between cloud cover and varT. The regression analysis of this relationship is presented in Fig. 3 and Table 3.

To assess whether the novel approach of estimating $K^{\downarrow}$ was useful for urban heat modelling, the approach was compared with the model results where observed radiation was used as driver. The first step was to replace the observations with varT data. The resulting model outputs of Q_e and Q_h were compared between the two approaches. Fig. 6 is an illustrative example, whereas Table 4 and Fig. 5 depict the results for the entire dataset.

Table 3
Overview of regression model properties in Eq. (2) for "all" and "dry" (hours without rain at Amsterdam Airport) conditions. The sections contain the complete model overview, the regression coefficients and the 95% confidence intervals, and the median absolute error (MedAE) respectively. For the latter, a subset of N_{sub} randomly selected data (50%) points is used to create regression coefficients and MedAE in Wm^{-2} is calculated from the remaining data and Eq. (1b).

	Complete model				Regression coefficients				MedAE	
					γ		δ			
	N	df.	$RMSE$	R^2_{adj}	est.	95%	est.	95%	N_{sub}	Wm^{-2}
all	3684	3682	0.219	0.502	0.677	±0.011	−0.257	±0.009	1892	55.1
dry	3119	3117	0.200	0.515	0.634	±0.012	−0.248	±0.009	1616	47.1

The varT model shows similar results to the model fed with professionally observed radiation data (referred to as "Meteo model"). For some days, the varT model even outperforms the meteo model, e.g. on June 1st and 2nd. On these days, the varT model more accurately recognises the cloudy conditions and adjusts the heat fluxes accordingly.

The predicted time series are significantly correlated to the observed time series in all cases (Table 4). Also when Q_e and Q_h are summed to find the total available energy (Q_a), the relation is significant. The median absolute error (MedAE) values show that the varT model outperforms the Meteo model for all three fluxes, showing on 35% decrease in the MedAE averaged over all three flux types.

Results for the normalised MedAE (Table 4), indicate that both models predict Q_h more accurately than Q_e, because the MedAE value is lower in both the Meteo and the varT model. Also, the Q_a is more accurately estimated than the individual fluxes, signalling that the partitioning of Q_e and Q_h is challenging for the model.

4. Discussion

Here we compare our model scores with reported model scores in the literature. Hanna and Chang [32] evaluated the daytime Q_h estimates of the Hybrid Plume Dispersion Model using observations in Saint Louis (Missouri, USA) and Indianapolis (Indiana, USA). They found a RMSE of 20–50 Wm^{-2} and an nRMSE of 0.20–0.50. Hence our results for the daytime period ($K^{\downarrow} > 120$ Wm^{-2}) are in line with their results (Table 5). Grimmond and Oke [33] evaluated the LUMPS model for North-American cities, and found a RMSE of 42 Wm^{-2} and 27

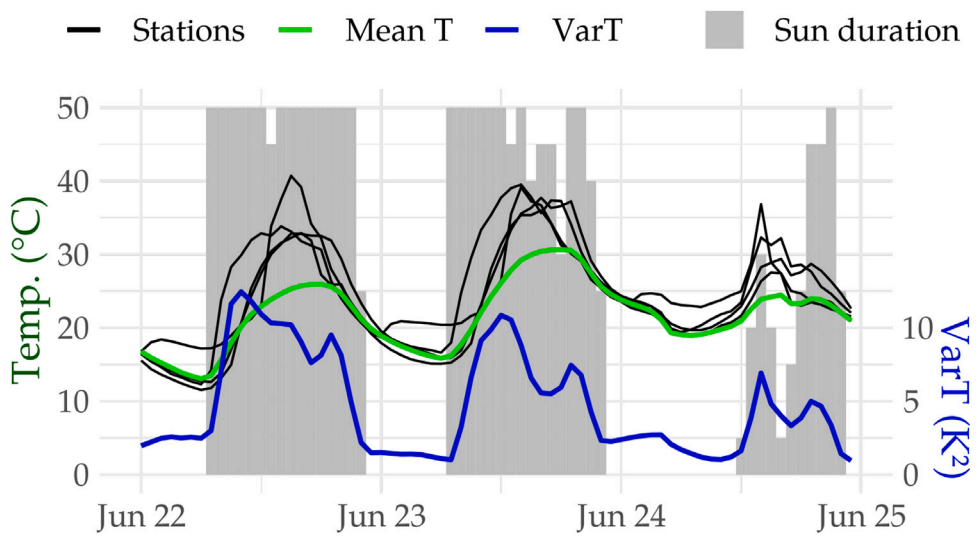

Fig. 4. Illustration of the relation between observed hourly sun duration (grey) and varT (blue) for 22–25 June 2022. Black lines correspond to the four Netatmo stations that observed the highest maximum temperature on June 22nd, and are suspected radiation-biased stations. The green line indicates the mean temperature of all Netatmo stations in the network. (For interpretation of the references to colour in this figure legend, the reader is referred to the web version of this article.)

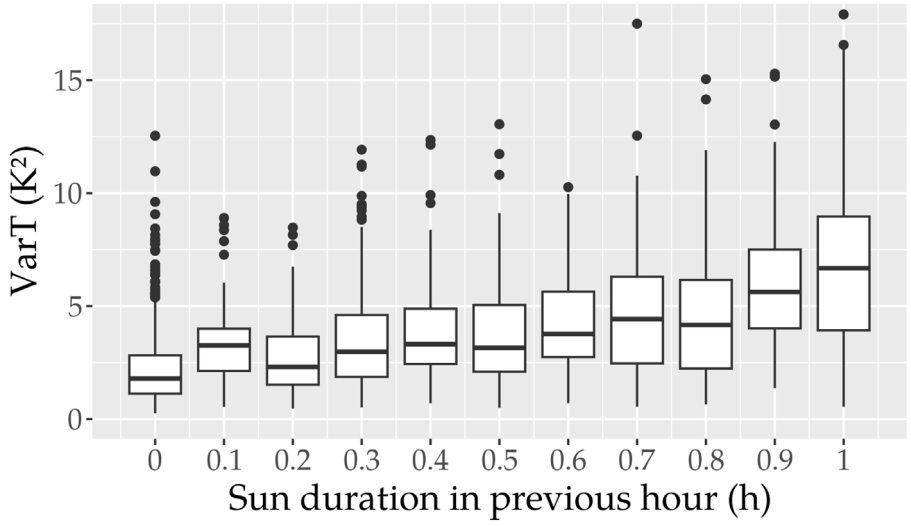

Fig. 5. Boxplots of observed varT of all Netatmo stations in a 10 km radius around the Amsterdam airport weather station (N = 136) versus the sunshine duration as a fraction of the total possible duration. The horizontal axis shows discrete sunshine duration values, ranging from 0 (completely overcast in the previous hour) to 1 (completely sunny) observed at Amsterdam airport. The period is March 1st to August 31st 2022 and one value is plotted per daytime hour (2832 entries).

Table 4
Overview of Pearson's product-moment correlation of Q_e, Q_h and Q_a in Amsterdam. The time frame is March 1 to August 31 of 2020, and one entry is presented per half hour for non-rainy hours with observations of the relevant heat flux. Q_a was only used when both Q_e and Q_h were available. Column MedAE shows the median absolute error for each flux (absolute and normalised (*norm.*)).

		Pearson's product-moment correlation					MedAE	
		N	*d f.*	*r*	*t*	*p*-value	Wm^{-2}	*norm.*
Meteo model	Q_e	2664	2662	0.465	27.1	≪0.0001	22.8	0.629
	Q_h	3899	3897	0.783	78.7	≪0.0001	46.3	0.461
	Q_a	2222	2220	0.873	84.3	≪0.0001	55.4	0.449
varT model	Q_e	2666	2664	0.473	27.7	≪0.0001	17.5	0.500
	Q_h	3901	3899	0.749	70.6	≪0.0001	30.5	0.304
	Q_a	2223	2221	0.843	74.0	≪0.0001	33.2	0.269

Wm^{-2} for Q_h and Q_e respectively. Hence our model (Fig. 2(a)) performs slightly better for Q_h, while for Q_e LUMPS performs best. Nevertheless, note the described errors for LUMPS are a summary for twelve datasets, collected in seven cities with surface characteristics and climates that differ from Amsterdam. Concerning the model score for u_*, we compare with results from Roulet et al. [58] for four consecutive summer days in Basel (Switzerland), using the [59] scheme. Their RMSE of 0.09 ms^{-1}, is close to our RMSE of 0.11 ms^{-1}.

Despite the potential of crowdsourcing data [60], they have not been used so far as input for flux estimation models. Quality assessments of Netatmo setups found that temperature difference are within ±0.5 K for the afternoon, evening and night, whereas in the morning the Netatmo sensors underestimated T_{air} by 0.5–1.3 K [16]. Contrarily, Chapman et al. [6] found a warm bias of 0.73 K on neighbourhood-scale in London (U.K.). Fenner et al. [61] found generally higher mean temperatures measured by the Netatmo PWSs than by the professional stations in Berlin (Germany). A sensitivity test on the average temperature effect revealed that a bias +0.5 and −1 K result in a mean Q_H difference of 0.15 Wm^{-2} and 0.17 Wm^{-2} respectively. For Q_E the range is between 1 Wm^{-2} and no substantial impact is seen for u_*.

In our approach, the best $K^{\downarrow}$ estimation is achieved when modelling the fraction of $K^{\downarrow}$ that is blocked by cloud cover. This method accounts

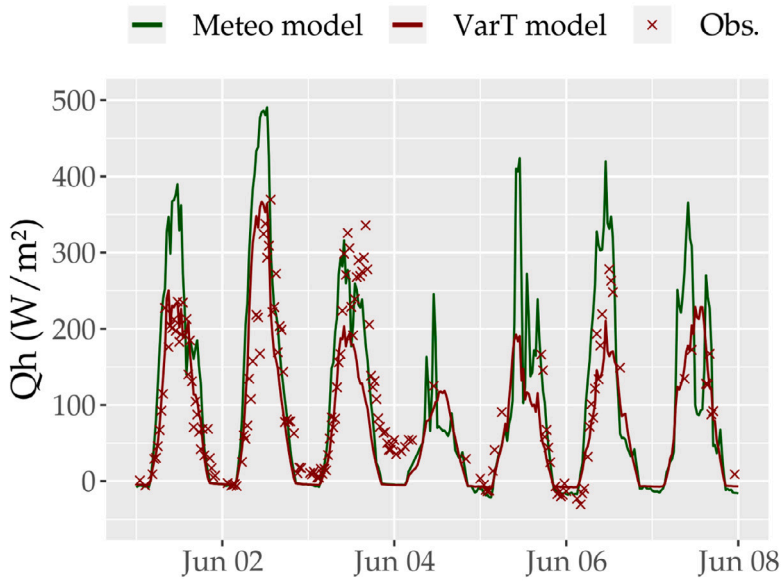

(a) **Sensible heat flux**

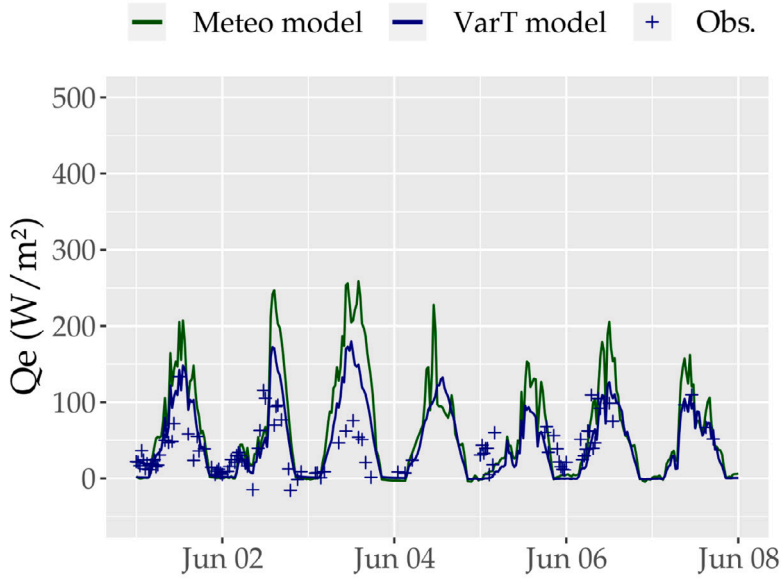

(b) **Latent heat flux**

Fig. 6. Time series of urban heat fluxes Q_h and Q_e in the first week of June 2020. Meteo model was fed with radiation data from the Amsterdam airport professional weather station, VarT model with radiation data generated from Netatmo stations. Green line indicates model results produced by the meteo model. Observations of both fluxes are indicated with markers. (For interpretation of the references to colour in this figure legend, the reader is referred to the web version of this article.)

for the daily and yearly fluctuations in $K^{\downarrow}_{cs}$ depending on site location and is thus transferable to other cities. This suggests varT of urban Netatmo datasets can be used to model $K^{\downarrow}$ with substantial accuracy.

A certain level of accuracy of the varT approach was shown at a sample size of 81 Netatmo stations. This implies that the dataset showed enough variability in stations when N was its lowest value of 95. In this study, we visually classified 11 stations as radiation-biased stations. This is in line with previous studies using systematic approaches for filtering by Meier et al. [16] and Fenner et al. [37], where approximately 10% of Netatmo observations were discarded for radiation biases. Here we estimate that $N \gtrsim 40$ ($\sim 1\text{km}^{-2}$) is sufficient for $K^{\downarrow}$ estimations, which seems an acceptable rule-of-thumb for future analyses. Increasing the sample size beyond 40 does not yield higher accuracy $K^{\downarrow}$ estimations, but it does benefit the certainty of the model as a larger sample size increases the likelihood that sufficient radiation-biased stations are present. Further testing on the need of data density and composition over the city is recommended on larger cities than Amsterdam.

When applying the regression parameters of Amsterdam to datasets in Tokyo and Vienna, similar results were acquired for the two cities, indicating that this relation is more widely applicable, which strengthens the confidence in our approach. The regression analyses for Tokyo and Vienna showed similar results for parameters γ and δ as in Amsterdam. We therefore recommend $\gamma = 0.70$ and $\delta = -0.25$ for subsequent analyses in other cities.

Table 5
Overview error statistics.

Experiment	flux	r^2	RMSE	nRMSE	bias	MAE	MedAE	$mean_{obs}$	$mean_{model}$
All data	Q_H (Wm^{-2})	0.80	44.0	0.53	−0.4	29.4	19.2	82.7	82.3
No precip	Q_H (Wm^{-2})	0.84	38.8	0.44	−2.7	27.6	18.6	89.1	86.4
Daytime only	Q_H (Wm^{-2})	0.65	50.8	0.31	−2.3	38.5	30.6	163.1	160.8
All data	Q_E (Wm^{-2})	0.15	48.6	1.30	−13.7	27.1	15.2	37.5	23.8
No precip	Q_E (Wm^{-2})	0.28	34.6	0.94	−12.8	22.1	14.3	37.0	24.5
Daytime only	Q_E (Wm^{-2})	0.06	46.7	0.80	−13.6	29.9	19.3	58.1	44.6
All data	u_* (ms^{-1})	0.75	0.27	0.47	0.19	0.21	0.16	0.59	0.77
No precip	u_* (ms^{-1})	0.76	0.25	0.45	0.18	0.19	0.16	0.55	0.73
Daytime only	u_* (ms^{-1})	0.66	0.25	0.39	0.16	0.19	0.15	0.63	0.80

Besides direct radiation, varT can also arise from precipitation, leading to discrepancies in the varT approach proposed here. In our dataset rainy hours show a higher varT, while a relatively low varT is expected in overcast scenarios. Precipitation has a cooling effect [62], and spatial variance in T_{air} can also appear when there is spatial variation in precipitation (e.g. rain showers). This may create spatial differences in evapotranspiration, and thus in temperature. In those cases, varT does not only indicate $K^{\downarrow}$ and is thus not of use to the model. For future analyses, rainy hours should be excluded from the varT approach. These results are contradicted by Potgieter et al. [63], who observed a smaller variance in Netatmo datasets on days with precipitation, presumably caused by thick cloud cover on rainy days. More evaluations are needed to understand the relation between rainfall and temperature observations of the Netatmo network.

Moreover, Venter et al. [35] used Netatmo data as spatial inputs to model the micro-meteorology of Oslo (Norway), and noted as well that varT increases with increasing global radiation, but they attribute this increase to an increase in hyperlocal variability on hot, calm days. On the other hand Meyer et al. [42] has attributed increased varT to the passively ventilated aluminium casing of the Netatmo sensor. In addition, Netatmo sensor can be affected by longwave radiation emitted from nearby warm walls that are exposed to the solar radiation as well. More arguments were provided to assume siting differences to be the most likely cause, as the temperature deviations are too large to represent an actual spatial variance within the relatively small study area. If it is assumed that differences can be attributed solely to the direct sun exposure of erroneously placed temperature sensors, the varT-$K^{\downarrow}$ relation seems reasonable.

Overall, the varT approach has been shown to be able to model $K^{\downarrow}$ using only Netatmo data and coordinates. This is a major improvement from previous versions of the model, which always required additional radiation observations. This implies that an indication of $K^{\downarrow}$ can be generated from Netatmo data alone, which is suitable for urban heat flux modelling.

In addition, we note that the varT model overall generates smoother outputs than the meteo model for both the sensible heat flux (Fig. 6(a)) and the latent heat flux (Fig. 6(b)). This is caused by a certain inertia that is present in the varT, being dependent on a larger area, whereas meteorological observations are indicative of a single location. This is a beneficial behaviour for the flux model, since the model is built to represent the fluxes on a neighbourhood scale, which should not be reliant on quickly shifting point observations.

Our study is limited in that the prevailing large-scale wind direction is not taken into account, although this may affect the footprint area of the turbulent flux. On microscale and local scale, wind characteristics are highly variable due to aerodynamic and thermal effects [64]. For example, buildings and other roughness elements of variable size distort the air flow and differences in thermal properties between surface cover types or fabric may lead to (intra-urban) advection when temperature differences become large enough. Thus, because of the heterogeneity of the urban surface, differences in wind behaviour can be observed between source areas. The wind characteristics for the flux site for May 2018 to August 2022, we find the most frequently occurring direction was south (19%), closely followed by southwest (18%), which is the prevailing wind direction in the Netherlands.

Here we report on model experiments in which the observed wind direction at the AAMS flux tower is used to determine the wind sector (8 wind sectors of 45°) that acts as the source area of the flux estimates. Only Netatmo stations present in the wind sector were used for flux estimates. In our metrics only the time steps where flux output of both the wind sector experiments and reference experiments are available are included. Note that in some wind sectors only 1 or 2 wind sensors were available. We find that the Q_H estimate of are slightly better when wind direction is taken into account. In general, the over- and underestimations are weaker, particularly when the flux is larger (> 100 Wm^{-2}). r^2 is somewhat higher for the wind sector run (r^2 = 0.85) than for the reference run (r^2 = 0.84). Also the RMSE and nRMSE indicate model when wind direction is considered, since they are 2.0 Wm^{-2} and 0.02 smaller than for the reference experiment. Contrarily, Q_E estimates do not improve when the wind sector experiment compared to the reference experiment. Most remarkable, however, is the model performance for u_* when wind direction is taken into account. The wind sector estimates of u_* do not match the observations well (r^2 = 0.24). The RMSE amounts to 0.34 ms^{-1}, which is three quarters of the mean observed flux, and more than three times the RMSE as found for the reference experiment. Hence, taking into account wind direction limits the number of wind sensors in the footprint and generated has mixed results, and therefore was not explored further here.

This paper represents a proof-of-principle for modelling urban heat fluxes from crowdsourced data alone. As there is a high data availability of Netatmo sensors worldwide [15,65–67], there is a great potential to apply the model scheme to different urban areas. This means that first order estimates of the urban heat fluxes can be estimated relatively easily for a variety of cities, without the direct need for professional local observations. At the same time, Fig. 2(a) also indicates there is room for improvement by reducing bias and scatter further. Herein a wider availability of multiple flux stations across the city might be beneficial to evaluate how much spatial flux variation can be expected.

5. Conclusion

This paper presents a novel method to estimate urban turbulent fluxes only from crowdsourced in situ observations (Netatmo weather stations) in the urban canyon. The approach is evaluated in the Amsterdam Atmospheric Monitoring Supersite in The Netherlands. First we extend the flux estimation scheme by Holtslag and Van Ulden [30] by implementing the Objective Hysteresis Model [50] to account for the storage heat flux in the urban environment. Second we account for the roughness sublayer effects using a wind speed and temperature profile parameterisation within the canyon [56,68]. The scheme requires incoming solar radiation ($K^{\downarrow}$), air temperature (T_{air}), wind speed (u), relative humidity (RH), air pressure (p) and cloud cover (N) as input, and information about urban surface properties and morphology.

Moreover, we substituted professionally observed $K^{\downarrow}$ with crowdsourced $K^{\downarrow}$ estimates. We show that the local $K^{\downarrow}$ can be estimated from the spatial variance in crowdsourced temperature observations triggered by directly irradiated Netatmo sensors. A straightforward regression of the logarithm of the spatial temperature variance was shown to successfully estimate $K^{\downarrow}$. This relation applies to Amsterdam,

but model regression parameters could be successfully transferred to Tokyo and Vienna, indicating that the approach has a potential for a wider applicability.

Overall, we show the potential of estimating turbulent fluxes and $K^{\downarrow}$ using only crowdsourced observations, which can serve cities where professional observations are lacking, but that do contain ~ 40 or more Netatmo stations. Urban heat flux models fed with these data can offer relatively rapid insights into the mechanics of heat fluxes in cities.

CRediT authorship contribution statement

W. van der Meer: Writing – review & editing, Writing – original draft, Software, Methodology, Investigation, Formal analysis, Conceptualization. **F. Zantinge:** Writing – original draft, Visualization, Validation, Software, Methodology, Investigation, Formal analysis, Conceptualization. **G.J. Steeneveld:** Writing – review & editing, Supervision, Project administration, Methodology, Investigation, Funding acquisition, Formal analysis, Conceptualization.

Declaration of competing interest

We wish to confirm that there are no known conflicts of interest associated with this publication and there has been no significant financial support for this work that could have influenced its outcome.

Acknowledgements

G.J. Steeneveld acknowledges funding from the Dutch Research Council (NWO, grant 864.14.007), and from the 4TU-program HERITAGE (HEat Robustness In relation To AGEing cities), funded by the High Tech for a Sustainable Future (HTSF) program of 4TU, the federation of the four technical universities in The Netherlands. The Amsterdam Atmospheric Monitoring Supersite (AAMS) has been financially supported by the Amsterdam Institute for Advanced Metropolitan Solutions (grant VIR16002). The AAMS is part of the Ruisdael Observatory, a scientific research infrastructure which is (partly) financed by the Dutch Research Council (NWO, grant 184.034.015). The authors thank Bradley Matthews and Enrichetta Fasano (Boku university, Vienna) for fruitful discussions on the method and data, and Bert Heusinkveld (WU) for his continuous efforts on the flux observations in AAMS. We thank two anonymous reviewers for their feedback on the original manuscript.

Data availability

The flux data in the AAMS network are available via https://maq-observations.nl/data-downloads/ and the KNMI data for Amsterdam airport are available via https://www.knmi.nl/nederland-nu/klimatologie/uurgegevens. Netatmo data have been gathered via an API that is available through https://dev.netatmo.com/apidocumentation/weather#getstationsdata, under the license conditions present at https://dev.netatmo.com/legal.

References

[1] United Nations. World cities report 2022: Envisaging the future of cities. New York: United Nations; 2022, p. 15, 978-92-1-132894-3, https://unhabitat.org/world-cities-report-2022-envisaging-the-future-of-cities.

[2] IPCC. Climate change 2022: Mitigation of climate change. Contribution of working group III to the sixth assessment report of the intergovernmental panel on climate change. Cambridge University Press; 2022, http://dx.doi.org/10.1017/9781009157926.

[3] Stewart ID. A systematic review and scientific critique of methodology in modern urban heat island literature. Int J Climatol 2011;31(2):200–17.

[4] Kousis I, Pigliautile I, Pisello AL. Intra-urban microclimate investigation in urban heat island through a novel mobile monitoring system. Sci Rep 2021;11(1):1–17.

[5] Vargas Zeppetello LR, Raftery AE, Battisti DS. Probabilistic projections of increased heat stress driven by climate change. Commun Earth & Environ 2022;3:183. http://dx.doi.org/10.1038/s43247-022-00524-4.

[6] Chapman L, Bell C, Bell S. Can the crowdsourcing data paradigm take atmospheric science to a new level? A case study of the urban heat island of London quantified using Netatmo weather stations. Int J Climatol 2016;37:3597–605.

[7] Muller CL, Chapman L, Grimmond CSB, Young DT, Cai X. Sensors and the city: a review of urban meteorological networks. Int J Climatol 2013;33(7):1585–600. http://dx.doi.org/10.1002/joc.3678.

[8] Peerlings E, Vranic S, Ommer J, Kalas M, Steeneveld GJ. Indoor heat in Amsterdam: Comparing observed indoor air temperatures from a professional network and from a citizen science approach. City Environ Interactions 2024;24:100173. http://dx.doi.org/10.1016/j.cacint.2024.100173.

[9] Chapman L, Bell C, Bell S. Can the crowdsourcing data paradigm take atmospheric science to a new level? A case study of the urban heat island of London quantified using Netatmo weather stations. Int J Climatol 2017;37(9):3597–605.

[10] WMO. Guide to instruments and methods of observation: Volume I –measurement of meteorological variables. Geneva; 2021.

[11] Oke TR. The urban energy balance. Prog Phys Geogr 1988;12(4):471–508.

[12] Stewart ID, Oke TR. Local climate zones for urban temperature studies. Bull Am Meteorol Soc 2012;93(12):1879–900.

[13] Rocha AD, Vulova S, Förster M, Gioli B, Matthews B, Helfter C, et al. Unprivileged groups are less served by green cooling services in major European urban areas. Nat Cities 2024;1(6):424–35. http://dx.doi.org/10.1038/s44284-024-00077-x.

[14] Zumwald M, Knüsel B, Bresch DN, Knutti R. Mapping urban temperature using crowd-sensing data and machine learning. Urban Clim 2021;35:100739.

[15] Coney J, Pickering B, Dufton D, Lukach M, Brooks B, Neely III RR. How useful are crowdsourced air temperature observations? An assessment of Netatmo stations and quality control schemes over the United Kingdom. Meteorol Appl 2022;29(3):e2075.

[16] Meier F, Fenner D, Grassmann T, Otto M, Scherer D. Crowdsourcing air temperature from citizen weather stations for urban climate research. Urban Clim 2017;19:170–91.

[17] Napoly A, Grassmann T, Meier F, Fenner D. Development and application of a statistically-based quality control for crowdsourced air temperature data. Front Earth Sci 2018;6:118.

[18] Beele E, Reyniers M, Aerts R, Somers B. Quality control and correction method for air temperature data from a citizen science weather station network in Leuven, Belgium. Earth Syst Sci Data 2022;14(10):4681–717.

[19] Droste AM, Heusinkveld BG, Fenner D, Steeneveld G-J. Assessing the potential and application of crowdsourced urban wind data. Q J R Meteorol Soc 2020;146(731):2671–88.

[20] Chen J, Saunders K, Whan K. Quality control and bias adjustment of crowdsourced wind speed observations. Q J R Meteorol Soc 2021;147(740):3647–64.

[21] De Vos L, Leijnse H, Overeem A, Uijlenhoet R. The potential of urban rainfall monitoring with crowdsourced automatic weather stations in Amsterdam. Hydrol Earth Syst Sci 2017;21:765–77.

[22] de Vos LW, Leijnse H, Overeem A, Uijlenhoet R. Quality control for crowdsourced personal weather stations to enable operational rainfall monitoring. Geophys Res Lett 2019;46(15):8820–9. http://dx.doi.org/10.1029/2019GL083731, URL https://agupubs.onlinelibrary.wiley.com/doi/abs/10.1029/2019GL083731. arXiv:https://agupubs.onlinelibrary.wiley.com/doi/pdf/10.1029/2019GL083731.

[23] Bárdossy A, Seidel J, El Hachem A. The use of personal weather station observations to improve precipitation estimation and interpolation. Hydrol Earth Syst Sci 2021;25(2):583–601. http://dx.doi.org/10.5194/hess-25-583-2021, URL https://hess.copernicus.org/articles/25/583/2021/.

[24] Overeem A, Leijnse H, van der Schrier G, van den Besselaar E, Garcia-Marti I, de Vos LW. Merging with crowdsourced rain gauge data improves pan-European radar precipitation estimates. Hydrol Earth Syst Sci 2024;28(3):649–68. http://dx.doi.org/10.5194/hess-28-649-2024, URL https://hess.copernicus.org/articles/28/649/2024/.

[25] Steeneveld G, Koopmans S, Heusinkveld B, van Hove L, Holtslag A. Quantifying urban heat island effects and human comfort for cities of variable size and urban morphology in the Netherlands. J Geophys Res 2011;116(D20129).

[26] Overeem A, Robinson RJC, Leijnse H, Steeneveld G-J, Horn PBK, Uijlenhoet R. Crowdsourcing urban air temperatures from smartphone battery temperatures. Geophys Res Lett 2013;40(15):4081–5.

[27] Mahoney WP, O'Sullivan JM. Realizing the potential of vehicle-based observations. Bull Am Meteorol Soc 2013;94(7):1007–18.

[28] Nadeau D, Girard P, Overby M, Pardyjak E, Stoll R, Willemsen P, et al. Validation of a fast-response urban micrometeorological model to assess the performance of urban heat island mitigation strategies. In: AGU fall meeting abstracts. vol. 2015, 2015, p. B33E–0765.

[29] De Vos LW, Droste AM, Zander MJ, Overeem A, Leijnse H, Heusinkveld BG, et al. Opportunistic sensing networks. Bull Am Meteorol Soc 2020;101(4):313–8.

[30] Holtslag AAM, Van Ulden AP. A simple scheme for daytime estimates of the surface fluxes from routine weather data. J Appl Meteorol Clim 1983;22(4):517–29.

[31] De Rooy WC, Holtslag AAM. Estimation of surface radiation and energy flux densities from single-level weather data. J Appl Meteorol 1999;38(5):526–40.
[32] Hanna S, Chang J. Boundary-layer parameterization for applied dispersion modeling over urban areas. Bound-Layer Meteorol 1992;58:229–59.
[33] Grimmond CSB, Oke TR. Turbulent heat fluxes in urban areas: Observations and a local-scale urban meteorological parameterization scheme (LUMPS). J Appl Meteorol Clim 2002;41(7):792–810.
[34] Google Earth Pro version 73610201. (2025) Last acesssed 11 Feb 2025.
[35] Venter ZS, Brousse O, Esau I, Meier F. Hyperlocal mapping of urban air temperature using remote sensing and crowdsourced weather data. Remote Sens Environ 2020;242:111791.
[36] Nakamura R, Mahrt L. Air temperature measurement errors in naturally ventilated radiation shields. J Atmos Ocean Technol 2005;22(7):1046–58.
[37] Fenner D, Bechtel B, Demuzere M, Kittner J, Meier F. CrowdQC+—a quality-control for crowdsourced air-temperature observations enabling world-wide urban climate applications. Front Environ Sci 2021;9:553.
[38] Ronda R, Steeneveld G, Heusinkveld B, Attema J, A.A.M. H. Urban finescale forecasting reveals weather conditions with unprecedented detail. Bull Am Meteorol Soc 2017;98:2675–88.
[39] Jansen FA, Jongen HJ, Jacobs CM, Bosveld FC, Buzacott AJ, Heusinkveld BG, et al. Land cover control on the drivers of evaporation and sensible heat fluxes: An observation-based synthesis for the Netherlands. Water Resour Res 2023. e2022WR034361.
[40] LI-COR Biosciences. EddyPro Software Instruction Manual. 2021.
[41] Lipson M, Grimmond S, Best M, Chow WT, Christen A, Chrysoulakis N, et al. Harmonized gap-filled datasets from 20 urban flux tower sites. Earth Syst Sci Data 2022;14(11):5157–78.
[42] Meyer L, Gubler MR, Meier F, Brönnimann S. Intercomparison and combination of low-cost urban air temperature measurement approaches. Meteorol Z 2021;31(2):131–48.
[43] Song T, Sun Y, Wang Y. Multilevel measurements of fluxes and turbulence over an urban landscape in Beijing. Tellus B: Chem Phys Meteorol 2013. http://dx.doi.org/10.3402/tellusb.v65i0.20421.
[44] Kasten F, Czeplak G. Solar and terrestrial radiation dependent on the amount and type of cloud. Sol Energy 1980;24(2):177–89.
[45] Perpiñán Lamigueiro O. solaR: solar radiation and photovoltaic systems with R. J Stat Softw 2012;50(9):1–32.
[46] Yap DH. Sensible heat fluxes measured in and near vancouver, BC [Ph.D. thesis], University of British Columbia; 1973.
[47] South C, Susan C, Grimmond B, Wolfe CP. Evapotranspiration rates from wetlands with different disturbance histories: Indiana Dunes National Lakeshore. Wetlands 1998;18:216–29.
[48] Doll D, Ching JKS, Kaneshiro J. Parameterization of subsurface heating for soil and concrete using net radiation data. Bound-Layer Meteorol 1985;32:351–72.
[49] Narita K. Thermal properties of urban surface materials. Study on heat balance at asphalt pavement. Geogr Rev Jpn Ser A 1984;57:639–51.
[50] Grimmond CSB, Cleugh HA, Oke TR. An objective urban heat storage model and its comparison with other schemes. Atmospheric Environ Part B. Urban Atmosphere 1991;25(3):311–26.
[51] Priestley CHB, Taylor RJ. On the assessment of surface heat flux and evaporation using large-scale parameters. Mon Weather Rev 1972;100(2):81–92.
[52] Kashyap PS, Panda RK. Evaluation of evapotranspiration estimation methods and development of crop-coefficients for potato crop in a sub-humid region. Agricult Water Manag 2001;50(1):9–25.
[53] Allen RG, Pereira LS, Raes D, Smith M. Crop evapotranspiration-Guidelines for computing crop water requirements-FAO Irrigation and drainage paper 56. Fao, Rome 1998;300(9):D05109.
[54] de Bruin HAR, Holtslag AAM. A simple parameterization of the surface fluxes of sensible and latent heat during daytime compared with the penman-Monteith concept. J Appl Meteorol Clim 1982;21(11):1610–21.
[55] Theeuwes NE, Ronda RJ, Harman IN, Christen A, Grimmond CSB. Parametrizing horizontally-averaged wind and temperature profiles in the urban roughness sublayer. Bound-Layer Meteorol 2019;173(3):321–48.
[56] Harman IN, Finnigan JJ. A simple unified theory for flow in the canopy and roughness sublayer. Bound-Layer Meteorol 2007;123:339–63.
[57] Macdonald RW, Griffiths RF, Hall DJ. An improved method for the estimation of surface roughness of obstacle arrays. Atmos Environ 1998;32(11):1857–64.
[58] Roulet Y-A, Martilli A, Rotach M, Clappier A. Validation of an urban surface eschange parameterization for mesoscale models - 1D case in a street canyon. J Appl Meteorol Clim 2005;44(9):1484–98.
[59] Martilli A. Numerical study of urban impact on boundary layer structure: sensitivity to wind speed, urban morphology, and rural soil moisture. J Appl Meteorol Clim 2002;41(12):1247–66.
[60] Muller C, Chapman L, Johnston S, Kidd C, Illingworth S, Foody G, et al. Crowdsourcing for climate and atmospheric sciences: current status and future potential. Int J Climatol 2015;35:3185–203.
[61] Fenner D, Meier F, Bechtel B, Otto M, Scherer D. Intra and inter 'local climate zone' variability of air temperature as observed by crowdsourced citizen weather stations in Berlin, Germany. Meteorol Z 2017;26(5):525–47.
[62] Liu W, Dong S, Zheng J, Liu C, Wang C, Shangguan W, et al. Quantifying the rainfall cooling effect: The importance of relative humidity in Guangdong, south China. J Hydrometeorol 2022;23(6):875–89.
[63] Potgieter J, Nazarian N, Lipson MJ, Hart MA, Ulpiani G, Morrison W, et al. Combining high-resolution land use data with crowdsourced air temperature to investigate intra-urban microclimate. Front Environ Sci 2021;9:385.
[64] Oke TR, Mills G, Christen A, Voogt JA. Urban climates. Cambridge University Press; 2017.
[65] van der Linden L, Hogan P, Maronga B, Hagemann R, Bechtel B. Crowdsourcing air temperature data for the evaluation of the urban microscale model PALM—A case study in central Europe. PlosClim 2023;8:e0000197. http://dx.doi.org/10.1371/journal.pclm.0000197.
[66] Romero Rodríguez L, Guerrero Delgado M, Castro Medina D, Sánchez Ramos J, Álvarez Domínguez S. Forecasting urban temperatures through crowdsourced data from Citizen Weather Stations. Urban Clim 2024;56:102021. http://dx.doi.org/10.1016/j.uclim.2024.102021, URL https://www.sciencedirect.com/science/article/pii/S2212095524002177.
[67] Bechtel B, Kittner J, Fenner D, Demuzere M. A global database of quality-controlled crowd weather station data. 2024, p. 1788. http://dx.doi.org/10.5194/egusphere-egu24-1788.
[68] Harman IN, Finnigan JJ. Scalar concentration profiles in the canopy and roughness sublayer. Bound-Layer Meteorol 2008;129:323–51.